Oscillatory Chemical Reaction in a CSTR with Feedback Control of Flow Rate

Milos Dolnik, Alexander S. Banks, and Irving R. Epstein*

Department of Chemistry and Center for Complex Systems, Brandeis University, Waltham, Massachusetts 02254-9110

Received: February 27, 1997; In Final Form: April 25, 1997[⊗]

We present an experimental and numerical study of the chlorine dioxide−iodide (CDI) reaction in a single, well-stirred, flow-through reactor with feedback regulation of flow rate in three different arrangements. The control is accomplished through a computer-mediated sigmoidal dependence of the dynamic flow rate(s) on the iodide concentration. Numerical simulations predict interesting dynamics in the CDI reaction system, which, without control, displays only steady-state and/or simple periodic oscillations. Our experiments confirm that bursting emerges as a result of the feedback control. We attribute bursting to the coexistence of the stable steady state and oscillations in the uncontrolled system. A period doubling sequence leading to chaos results from the nonlinear dependence of the oscillatory period on the flow rate in the vicinity of a Hopf bifurcation point.

Introduction

Addition of a feedback control mechanism to a chemical oscillator can stabilize unstable steady states[1−3] and periodic solutions.[4−6] In some cases the feedback control gives rise to quite new solutions, e.g., chaotic orbits.[7] Another behavior that can arise in controlled oscillatory systems is bursting, i.e., regular alternating periods of quiescence and of oscillations.[8,9] Bursting is a common behavior of neural oscillators and can occur in single isolated neurons or in networks of synaptically connected neurons. Recent data from stomatogastric ganglion neurons of spiny lobsters suggest that neurons regulate their conductances to maintain their stable activity patterns.[10] Abbott and co-workers[11−13] developed a Ca^{2+}-dependent regulation scheme to model the effects of cellular activity on conductances in single and multicompartment model neurons. Their mechanism allows model neurons to self-assemble and adjust their conductances to produce stable and robust patterns of activity.

Oscillating chemical reactions exhibit a wide range of dynamical phenomena that are also observed in other systems. They have therefore been considered good models for more complex biochemical and biological systems. We have recently suggested[14] the chlorine dioxide−iodide (CDI) reaction[15] in a continuously stirred tank reactor (CSTR) with feedback control as a model that mimics the control mechanism proposed for neurons.[11] As an indicator of activity of the CDI reaction, the analog of the neuron's intracellular Ca^{2+} concentration, we employed the iodide concentration. The flow rate was taken as the dynamical variable to be controlled, in analogy to a conductance in a neuron.

The behavior of the CDI reaction without computer control, i.e., at constant flow rate, depends upon the input iodide concentration and on the fixed flow rate. Five separate regions have been identified for this reaction (Figure 8 in ref 16): two steady states, with high (HI) and low iodide (LI) concentrations; a region of sustained oscillations; and two different types of bistability, one between HI and LI steady states, and the second between the HI steady state and sustained oscillations. The CDI reaction does not display bursting nor chaos if no feedback control is present.

In this paper, we first describe the experimental realization of the feedback control mechanism suggested in the previous work,[14] and we describe the implementation of two additional control schemes. Next, we present experimental and numerical examples of bursting behavior and other regimes observed in these systems. We analyze the conditions and parameters that play the most important roles in the dynamics of the controlled systems. In the discussion, we demonstrate how bursting behavior and chaos emerge in the CDI reaction with feedback control.

Experimental Section

(a) Experimental Arrangement. A thermostatted ($T = 25.0$ °C) plexiglass continuous-flow well-stirred tank reactor (CSTR) of volume 35 mL was used in all experiments. The input solutions of chlorine dioxide, potassium iodide, and sulfuric acid were delivered to the reactor from separate tubes without premixing. Rainin Rabbit Plus peristaltic pumps were used to infuse the solutions. Chlorine dioxide was prepared as described in ref 17; potassium iodide and sulfuric acid were both Fisher ACS certified reagents. The concentration of chlorine dioxide was determined spectrophotometrically ($\epsilon = 1260$ cm^{-1} M^{-1} at $\lambda = 358$ nm) before each experiment was started. During the experiments, the stock solution was immersed in a 0 °C bath to avoid evaporation of ClO_2 and to maintain kinetic stability. During the transfer to the reactor, the temperature of the ClO_2 solution increased to approximately room temperature. The dynamic variation of the flow rate in the experiments resulted in small temperature fluctuations of the solution inside the reactor. The largest observable fluctuations were not larger than ±0.4 °C. The concentration of iodide in the reactor was monitored with an iodide ion-selective electrode (ISE) and a calomel reference electrode attached to a digital voltmeter. The electrodes were calibrated weekly against iodide stock solutions ranging in concentration from 10^{-2} to 10^{-8} M.

We utilize three different schemes of dynamical control both in the experiments and in the simulations: (i) in setup A (Figure 1a), all reagents are delivered into the reactor by a single pump from separate tubes. Control is achieved by the negative feedback mechanism, which increases the flow rate when the iodide concentration inside the reactor is below the target concentration and vice versa. The control mechanism does not affect the ratio of initial reagents, only the overall flow rate k_0.

(ii) In setup B (Figure 1b), two independent pumps are used to feed the reactor with reagents: ClO_2 and H_2SO_4 solutions

[⊗] Abstract published in *Advance ACS Abstracts,* June 1, 1997.

S1089-5639(97)00728-7 CCC: $14.00

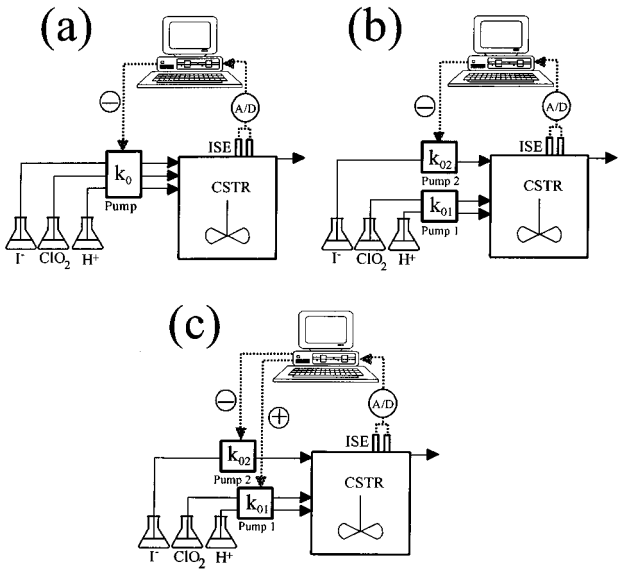

Figure 1. Experimental setups. The iodide concentration is estimated from the potential of an iodide ion-selective electrode (ISE) paired with a calomel reference electrode. The potential difference between the electrodes is measured with a voltmeter with analog to digital converter (A/D). Data are acquired by a computer which calculates the flow rate and controls the pump(s). (a) Setup A: reagents are delivered into the reactor by a single pump. Control is achieved by a negative feedback which increases the flow rate when the iodide concentration inside the reactor is low and *vice versa*. (b) Setup B: two pumps are used to feed the reactor: one pump has a constant flow rate, and the flow rate of the other pump (for the potassium iodide solution) is controlled by the computer. (c) Setup C: two pumps are used for feeding reagents, both with dynamical control. The flow of KI is controlled by a negative feedback, while the flow rate of an acidic solution of ClO_2 is controlled by a positive feedback.

are delivered at a constant flow rate k_{01} by the first pump, while the KI solution is delivered by the second pump at the variable flow rate k_{02}. Negative feedback is employed for dynamical control of flow rate k_{02}.

(iii) In setup C (Figure 1c), two independent pumps are utilized to introduce the reagents; both are computer-controlled. The flow of KI (k_{02}) is controlled by a negative feedback, while the flow rate of the ClO_2 and H_2SO_4 solutions (k_{01}) is controlled by a positive feedback.

The concentrations of stock solutions are the same for all three arrangements: $[ClO_2]_S = 3 \times 10^{-4}$ M, $[KI]_S = 11.4 \times 10^{-4}$ M, and $[H_2SO_4]_S = 3 \times 10^{-2}$ M. With identical tubes in setup A the input concentrations are equal to one third of the concentrations of stock solutions. In setups B and C the input concentrations depend upon the ratio k_{01}/k_{02}.

(b) Control Mechanism. We utilize here a control mechanism similar to that used previously in simulations.[14] The flow rate k_0 is made to be a slowly varying dynamic variable. This regulatory mechanism forces the system to establish a specific average concentration of iodide in the reactor. The feedback controls and maintains the desired average concentration of iodide I_T, which corresponds to a particular pattern of activity. In this way we build a simple chemical system that mimics the dynamic regulation in a neuronal system.[11]

The dynamic flow rate can vary between zero and a maximum value k_{max} according to the concentration of iodide in the reactor. The required change of the flow rate Δk_0 is evaluated according to

$$\tau\frac{\Delta k_0}{\Delta t} = f([I^-]) - k_0 = \frac{k_{max}}{1 + ([I^-]/I_T)^n} - k_0 \qquad (1)$$

where n is the exponent of the sigmoidal function f and τ is the time constant for flow rate change.

Once the empty reactor has been filled with reagents, the experimental control mechanism is initiated. The computer program calculates the iodide concentration inside the reactor $[I^-]$ using the electrode calibration curve. Following a time interval Δt of voltage sampling, the iodide concentration is sampled again, a new k_0 is calculated, and the computer adjusts the pump speed accordingly.

Equation 1 is used to determine the flow rate for setup A. A similar equation is used in setup B for evaluation of the flow rate k_{02}, with k_{02} replacing k_0 in eq 1 and k_{01} held constant. Setup C requires an additional equation for the positive feedback of the flow rate k_{01}:

$$\tau\frac{\Delta k_{01}}{\Delta t} = g([I^-]) - k_{01} = \frac{k_{max,1}}{1 + (I_T/[I^-])^n} - k_{01} \qquad (2)$$

where the maximum flow rates may differ for the two pumps, but the remaining parameters n and I_T are equal in the two flows.

Experimental Results

In order to understand better the behavior of this system, we began our investigation by exploring the roles of parameters Δt, n, and τ in eqs 1 and 2. As the time step Δt approaches zero, the difference equations become ordinary differential equations (ODEs). Our experimental measurements and the results of simulations reveal that there is no observable difference in dynamic behavior between the difference equations and the ODEs if Δt is smaller than 2 s. Therefore, in the experiments described below we choose $\Delta t = 1$ s.

The parameter n affects the slope of the sigmoidal function in eqs 1 and 2. For $n \gg 1$ the sigmoidal function f can be approximated by a step function: $f = k_{max}$ for $[I^-] < I_T$, $f = 0$ for $[I^-] > I_T$, and $f = k_{max}/2$ for $[I^-] = I_T$. The larger the value of n, the more strongly the system is forced to find dynamics with an average iodide concentration close to the target value. For $n > 2$, the control feedback and the behavior of the system are only slightly affected by increasing n. We choose $n = 5$ in our experiments and simulations, and we confirm by simulations that there is no significant change in dynamics when the parameter n is increased tenfold.

The time constant τ affects the rate of iodide-dependent modification of the flow rate. In analogy with neuron model simulations,[11-13] we assume that τ is large relative to the chemical relaxation times. This choice corresponds to a slow adaptation to changes in the extracellular environment. To speed up our experiments, we set $\tau = 1000$ s. We have verified both by experiments and simulations that the dynamics remains qualitatively similar for other τ ($\tau = 500$, 2000, 4000, 10 000 s).

Setup A. Figure 2 shows several examples of oscillatory behavior observed in setup A. The top part of each figure displays the variable flow rate, and the bottom part displays the measured difference between the potentials of the ISE and the calomel reference electrode. Higher iodide concentration corresponds to more negative potential difference. Initial transient periods are excluded from Figure 2, and each pattern is displayed for a duration of 1 h, during which all parameters are fixed. Figure 2a−d shows the dynamical behavior for four different target concentrations I_T. A 10-fold change in the target concentration does not result in significantly different behavior when I_T is changed from 1×10^{-6} to 1×10^{-7} M (Figure 2a,b). Bursting behavior remains similar, preserving three oscillations per burst for both target concentrations. However, the quiescent

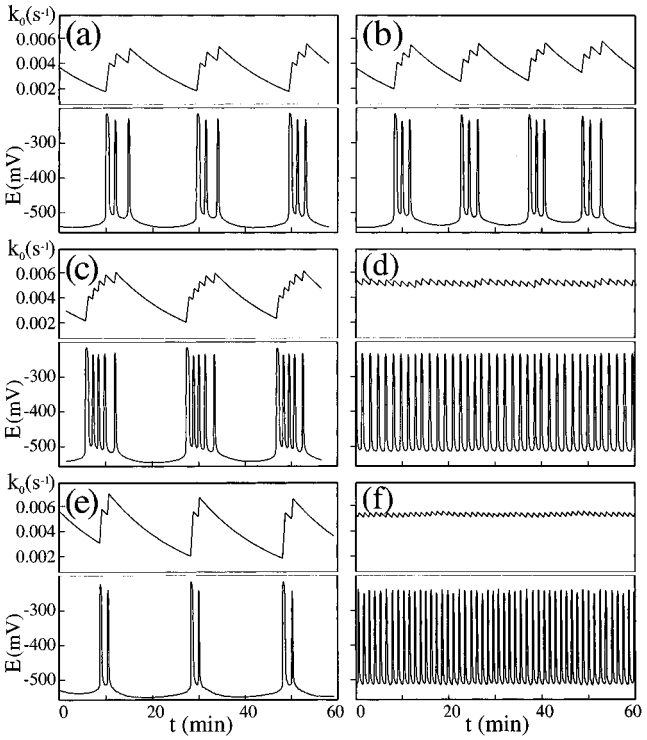

Figure 2. Dynamical behavior in setup A experiments: iodide (potential difference between electrodes, bottom part) and flow rate (top part) time series. Maximum flow rate k_{max}= 0.05 s^{-1} and target iodide concentration I_T = (a) 1×10^{-6} M, (b) 1×10^{-7} M, (c) 2×10^{-8} M, (d) 5×10^{-9} M. Target $I_T = 1 \times 10^{-6}$ M and k_{max} = (e) 0.1 s^{-1} (f) 0.025 s^{-1}.

period becomes shorter at smaller I_T. As the target concentration is further decreased, the number of oscillations per burst first increases (Figure 2c) until period-one oscillations, analogous to tonic firing in a neuron, emerge (Figure 2d). When I_T is set below the minimum value of the uncontrolled iodide concentration oscillations (not shown), the negative feedback holds the flow rate at a relatively low value at which only the low iodide steady state is sustained. To restore the oscillations, the target iodide concentration has to be increased to at least $I_T = 1 \times 10^{-7}$ M. This hysteresis indicates the coexistence of sustained oscillations and the stable LI steady state. There is no bistability for large values of I_T; when I_T is increased above 1×10^{-6} M the number of oscillations per burst decreases until low-frequency period-one oscillations emerge. Further increases of I_T yield only the high-iodide steady state, with a flow rate that approaches k_{max}.

A similar scenario of dynamical regimes is observed for fixed parameter I_T and variable k_{max} as shown in Figure 2a,e,f. For $I_T = 1 \times 10^{-6}$ M and $k_{max} = 0.1$ s^{-1}, bursting with two oscillations per burst represents a stationary pattern (Figure 2e). As k_{max} is decreased, the number of oscillations per burst increases much as it does when I_T is decreased, and eventually high-frequency period-one oscillations emerge for smaller k_{max} (Figure 2f). We obtain only the low iodide steady state for $k_{max} < 0.002$ s^{-1}. On the other hand, when k_{max} is increased above 0.1 s^{-1}, the bursting is replaced by low frequency period-one oscillations. These oscillations remain stable even for $k_{max} \gg 1$.

The flow rate k_0 varies significantly during a burst period. A roughly threefold change occurs in the flow rate during bursting in all experiments in setup A. High-frequency period-one oscillations are associated with smaller amplitude of the flow rate variation (Figure 2d). The amplitude increases with

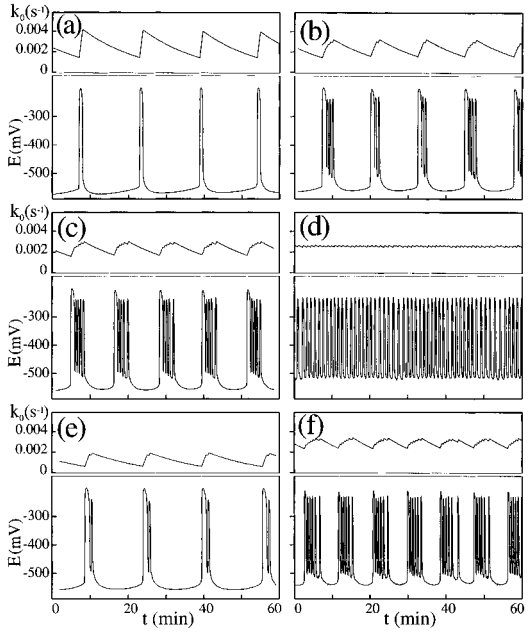

Figure 3. Dynamical behavior in setup B experiments: iodide and flow rate time series. Flow rate k_{01}= 0.005 s^{-1}, target concentration $I_T = 1 \times 10^{-6}$ M, and maximum flow rate k_{max} = (a) 0.05 and (b) 0.016 67 s^{-1}. k_{01}= 0.005 s^{-1}, k_{max}= 0.016 67 s^{-1}, and I_T = (c) 1×10^{-7} M, (d) 5×10^{-8} M. $I_T = 1 \times 10^{-6}$ M, k_{max}= 0.016 67 s^{-1}, and k_{01} = (e) 0.0025 s^{-1}, (f) 0.008 s^{-1}.

increasing period of iodide oscillations (see Figure 2d,f), a result that is explained in the Discussion.

Setup B. The scenario of dynamic regimes found in setup B resembles that in setup A. Figure 3 shows several examples. Figure 3a displays the behavior with the same control parameters as used in Figure 2a, but with the fixed flow rate $k_{01} = 0.005$ s^{-1}. Low-frequency period-one oscillations are the outcome of control in setup B, in contrast to the bursting oscillations in setup A. The period-one oscillations in setup B are preserved for a wide range of I_T, which indicates that for a similar set of parameters the control of dynamical behavior in setup B is more direct (and stronger) than in setup A. We weaken the effect of the control mechanism by reducing the parameter k_{max} by two-thirds and set $k_{max} = 0.01667$ s^{-1}. This choice reflects that in setup B the flow rate of only one out of three input species is dynamically varied. Figure 3b displays the bursting oscillations for $k_{max} = 0.01667$ s^{-1} and the other parameters as in Figure 3a. Changing I_T from 1×10^{-6} to 1×10^{-7} M has a relatively small effect on the bursting behavior (Figure 3b,c). As the target concentration is further decreased, the number of oscillations per burst continues to increase until the quiescent period disappears and high-frequency period-one oscillations emerge (Figure 3d). We also find here the coexistence of sustained oscillations and the stable LI steady state for small values of I_T ($I_T < 1 \times 10^{-7}$), but there is no bistability for large values of I_T.

Similar dynamical regimes are observed when we vary the time-independent flow rate k_{01}, as shown in Figure 3b,e,f. For $I_T = 1 \times 10^{-6}$ M and $k_{01} = 0.0025$ s^{-1} we observe bursting with two oscillations per burst (Figure 3e). As k_{01} becomes larger, the number of oscillations per burst increases as it does when we decrease I_T (Figure 3b,f), and eventually high-frequency period-one oscillations emerge for smaller $k_{01} > 0.01$ s^{-1}. Further increases in k_{01} yield the LI steady state.

The amplitude of oscillation of the flow rate k_{02} is smaller in setup B than in setup A. The amplitude decreases with decreasing k_{max}, and the time-averaged value $\langle k_{02} \rangle$ decreases with decreasing k_{01}. The average frequency of oscillations (spiking)

during a burst and the frequency of bursting are higher in setup B than in setup A.

Setup C. We employ here two independent feedbacks—negative feedback for the flow of the KI solution (eq 1) and positive feedback for the flow of the acidic solution of ClO_2 (eq 2). Figure 4a shows the transient and stationary behavior in this system with control parameters $k_{max,1} = k_{max,2} = 0.008\ 33\ s^{-1}$ and $I_T = 1 \times 10^{-6}$ M. The transient dynamics depends on the initial values of k_{01} and k_{02}. In Figure 4a, these are almost equal in the beginning. Because initially $[I^-] > I_T$, the flow of KI decreases and the flow of ClO_2 increases. During the period of high $[I^-]$ the ratio of $[ClO_2]_o/[I^-]_o$ increases, leading to the depletion of $[I^-]$ in the system and to the onset of oscillations.

During the oscillatory period the flow rate k_{02} oscillates with an increasing envelope, while the change in the flow rate k_{01} has the opposite sign. The resulting change in the ratio $[ClO_2]_o/[I^-]_o$ steers the dynamics once again toward the HI state and forms a single burst. After the transient period of approximately 30 min the change in $[ClO_2]_o/[I^-]_o$ is negligible, and the CDI reaction remains in a simple period-one oscillatory mode as if under constant flow in a CSTR. The negative and positive feedbacks change the individual flow rates in such a way that the total flow rate into the system follows a smooth trend without wavering through local minima and maxima.

We do not observe bursting for equal values of $k_{max,1}$ and $k_{max,2}$ when the flow rate $k_{01} < 0.01\ s^{-1}$. However, bursting arises as a result of unequal values of $k_{max,1}$ and $k_{max,2}$ as shown in Figure 4b,c. Figure 4b displays bursting behavior without the transient period for $I_T = 1 \times 10^{-5}$ and 1×10^{-6} M. As was the case in setups A and B, a 10-fold change in I_T does not produce a significant change in the bursting behavior.

Figure 4c illustrates the transient part after $k_{max,1}$ and $k_{max,2}$ are set to one-half of their previous value (compare with Figure 4b). Because the flow rate k_{01} is larger than the newly set parameter $k_{max,1}$, k_{01} decreases even for high $[I^-]$ in the reactor. After several bursts, the flow rate k_{01} drops below $k_{max,1}$. The flow rate k_{01} cannot exceed the parameter $k_{max,1}$ but must decrease if the initial value of k_{01} is above $k_{max,1}$. The ratio $k_{max,1}/k_{max,2}$ plays a more significant role in the dynamics than the absolute values of $k_{max,1}$ and $k_{max,2}$. When we change $k_{max,1}$ and $k_{max,2}$ while maintaining their ratio, the bursting persists with only slight changes (see Figure 4b,c).

Numerical Section

Model. The model of the CDI reaction proposed by Lengyel et al.[15] is based on two overall stoichiometric reactions:

$$ClO_2 + I^- \rightarrow ClO_2^- + \frac{1}{2}I_2 \qquad R_1 = k_1XY$$

$$ClO_2^- + 4I^- + 4H^+ \rightarrow Cl^- + 2I_2 + 2H_2O \qquad R_2 = k_{2a}ZYH + \frac{k_{2b}ZPY}{u + Y^2} \quad (3)$$

Here $X = [ClO_2]$, $Y = [I^-]$, $Z = [ClO_2^-]$, $P = [I_2]$, $H = [H^+]$, and R_i represent the rate laws. The rate constants and parameters used in the simulations are $k_1 = 6000\ M^{-1}\ s^{-1}$, $k_{2a} = 460\ M^{-2}\ s^{-1}$, $k_{2b} = 2.55 \times 10^{-3}\ s^{-1}$, $u = 1 \times 10^{-14}\ M^2$.

For a CSTR with an iodide-dependent flow rate of all input reagents (setup A, Figure 1a) the system of differential equations is

$$\frac{dX}{dt} = -R_1 + k_0(X_0 - X)$$

$$\frac{dY}{dt} = -R_1 - 4R_2 + k_0(Y_0 - Y)$$

$$\frac{dZ}{dt} = R_1 - R_2 - k_0Z \quad (4)$$

$$\tau\frac{dk_0}{dt} = \frac{k_{max}}{1 + (Y/I_T)^n} - k_0$$

$$P = \frac{Y_0 - Y}{2}$$

Here k_0 is the dynamic flow rate, which varies according to the concentration of iodide in the reactor, and X_0 and Y_0 are the input concentrations of X and Y. The feedback mechanism controls the speed of the input reagents flow into the CSTR while keeping the input concentrations constant. Because the input concentration of H^+ is high in comparison with that of the remaining species, we can neglect proton consumption in eq 3 and assume that $[H^+]$ inside the reactor is fixed at its initial concentration.

In setup B (Figure 1b) the input concentrations of all species vary with the ratio of the fixed flow rate k_{01} to the dynamical flow rate k_{02}, and we must consider $[H^+]$ to be a dynamical variable as well. The equations for setup B are

$$\frac{dX}{dt} = -R_1 + k_{01}X_s - k_0X$$

$$\frac{dY}{dt} = -R_1 - 4R_2 + k_{02}Y_s - k_0Y$$

$$\frac{dZ}{dt} = R_1 - R_2 - k_0Z$$

$$\frac{dH}{dt} = -4R_2 + k_{01}H_s - k_0H \quad (5)$$

$$\tau\frac{dk_{02}}{dt} = \frac{k_{max,2}}{1 + (Y/I_T)^n} - k_{02}$$

$$P = \frac{k_{02}Y_s - k_0Y}{2k_0}$$

$$k_0 = k_{01} + k_{02}$$

Here subscript s indicates concentration of the stock solutions, k_{01} is the fixed flow rate of ClO_2 and H_2SO_4, and k_{02} is the dynamical flow rate of iodide.

The mathematical model of setup C is described by the equations for setup B (eq 5) supplemented with the equation for the positive feedback of flow rate k_{01}:

$$\tau\frac{dk_{01}}{dt} = \frac{k_{max,1}}{1 + (I_T/Y)^n} - k_{01} \quad (6)$$

To analyze eqs 4, 5, and 6, we used the CONT numerical bifurcation and continuation package.[18] Periodic solutions were obtained by numerically integrating the system of ordinary differential equations. The integration used a semiimplicit

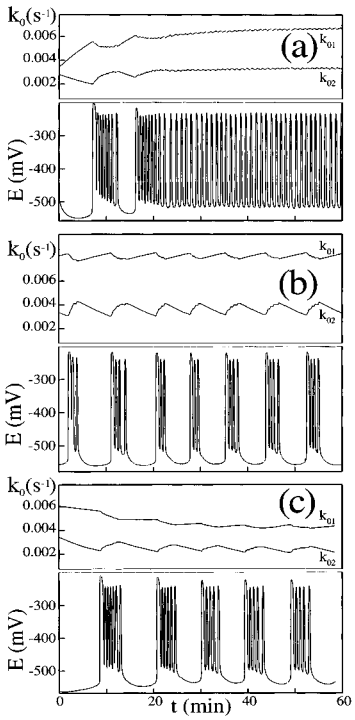

Figure 4. Dynamical behavior in setup C experiments: iodide and flow rate time series. (a) Maximum flow rates $k_{max,1} = k_{max,2} = 0.008\ 33$ s^{-1}, target iodide concentration $I_T = 1 \times 10^{-6}$ M. (b) $k_{max,1} = 0.008\ 33$ s^{-1}, $k_{max,2} = 0.016\ 66$ s^{-1}, $I_T = 1 \times 10^{-5}$ M (first half), 1×10^{-6} (second half). (c) $k_{max,1} = 0.004\ 16$ s^{-1}, $k_{max,2} = 0.008\ 33$ s^{-1}, $I_T = 1 \times 10^{-6}$ M.

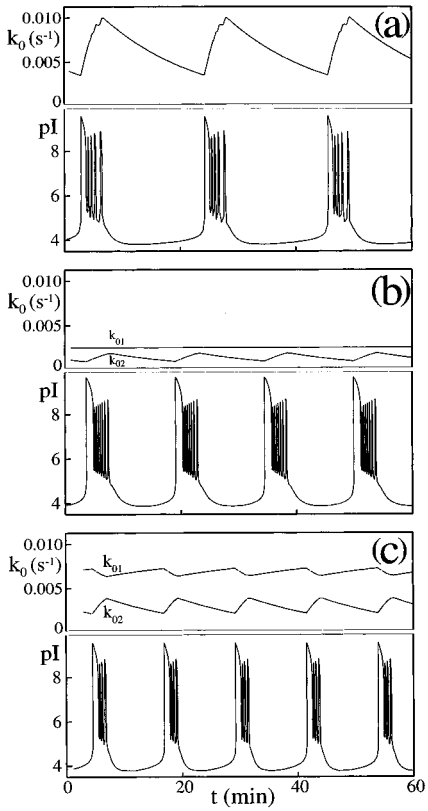

Figure 5. Bursting oscillations, simulations. (a) Setup A: target concentration $I_T = 1 \times 10^{-5}$ M, maximum flow rate $k_{max} = 0.05$ s^{-1}. (b) Setup B: $I_T = 1 \times 10^{-5}$ M, $k_{max} = 0.0166$ s^{-1}, fixed flow rate $k_{01} = 0.0025$ s^{-1}. (c) Setup C: $I_T = 1 \times 10^{-5}$ M, $k_{max,1} = 0.0083$ s^{-1}, $k_{max,2} = 0.0166$ s^{-1}.

fourth-order Runge−Kutta method with automatic control of the step size.

Results of Simulations

The model of the CDI reaction in a CSTR without feedback control shows good agreement with experiments.[8,9,16] Previous simulations[14] with the model of setup A revealed the presence of bursting and chaos. These results inspired the experimental investigation of the CDI reaction with feedback control. We performed additional numerical simulations to investigate the dynamics of setups A, B, and C. Models of these setups show bursting in simulations (Figure 5). Shown here are the iodide concentration ($pI = -\log_{10}[I^-]$) and the dynamically changing flow rates. Figure 5a displays bursting with five spikes per burst in setup A. During spiking, the flow rate increases sharply, and the maximum flow rate reaches nearly 3 times its minimum value. The flow rate increase is followed by a quiescent period during which the flow rate decrease is not as sharp as the previous increase. Bursting in setup B shows much smaller variations of the flow rate (Figure 5b). In setup C (Figure 5c) the opposite signs of the flow rate variations result in an almost constant total flow rate. The spiking in setups B and C has higher frequency than in setup A, as observed in our experiments.

We have studied in detail the dynamics of all setups as a function of the target concentration and the control parameter k_{max}. Figure 6 displays the bifurcation diagram of dynamic regimes for setup A as a function of the target concentration I_T when k_{max} is fixed at 0.05 s^{-1}. The diagram is obtained from a Poincaré map, with the flow rate k_0 evaluated at $[I^-] = 1 \times 10^{-7}$ M, for decreasing $[I^-]$. Figure 6a shows a full diagram with prevailing bursting behavior. The number of oscillations per burst decreases with increasing target concentration. Simple low-frequency period-one oscillations emerge just before the high value of the target concentration stabilizes the system at the HI steady state. We find similar scenarios for other values of k_{max} and also for models of setups B and C. In most simulations the chaotic oscillations are restricted to a relatively narrow parametric region, while regular bursting and simple periodic oscillations are widely present. Figure 6b shows a blowup of the diagram with the period doubling sequences leading to chaos. The chaotic region contains narrow periodic windows, including period-three and period-five windows with their own period doubling sequences. Bursting chaotic oscillations emerge at $I_T \approx 9 \times 10^{-7}$ M with increasing I_T. As I_T increases further, the bursting oscillations become periodic.

We summarize the results of simulations for setups A, B, and C in Figures 7 and 8. In these figures, the solid lines confine the entire oscillatory regions and the dashed lines represent subcritical Hopf bifurcation lines obtained from bifurcation analysis. Outside the solid lines the control mechanism always stabilizes the steady state. The steady state can also be stabilized for specific initial conditions outside the dashed lines. Shaded areas represent bursting; grey levels illustrate the number of spikes per burst. The black region is the domain of chaotic oscillations. Figure 7 shows that bursting is found only for intermediate values of k_{max} in all setups. The dynamics in these setups is qualitatively the same; from a quantitative point of view there is better agreement in the location of the bursting region between setups B and C (Figure 7b,c). The shape of the shaded areas suggests that the dynamics is almost independent of target concentration when $I_T \in (1 \times 10^{-7}, 1 \times 10^{-5})$ s^{-1}, while the strong dependence on k_{max} is apparent. Figure 8 demonstrates the close resemblance between setups B and C. The fixed flow rate k_{01} in setup B plays nearly the same role as the maximum flow rate $k_{max,1}$ in setup C. The variations of

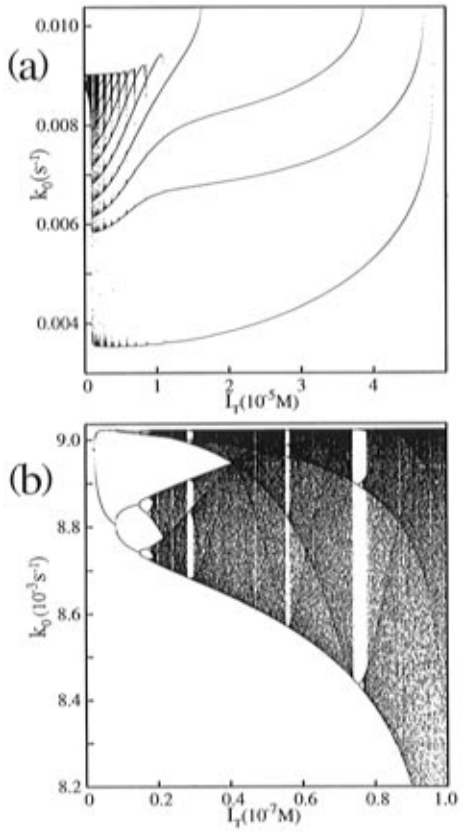

Figure 6. One-parameter bifurcation diagram—simulations for setup A. Points in the diagram correspond to values of flow rate k_0 on Poincaré surface: $Y = 1 \times 10^{-7}$ M, $k_{max} = 0.05$ s^{-1}. Small numbers of points correspond to periodic oscillations, while many points indicate chaos. (a) Full diagram with prevailing bursting behavior, (b) detail of diagram with chaotic oscillations.

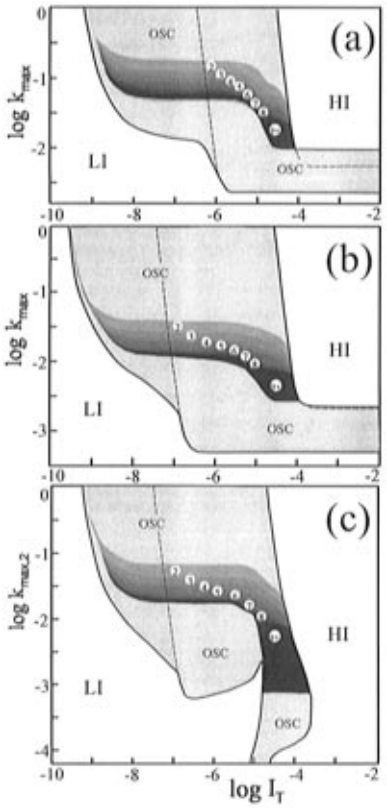

Figure 7. Bifurcation diagrams, simulations; Dashed line, Hopf bifurcation line; area confined by solid line, region of oscillations. Dark gray shaded area with numbers, bursting oscillations; gray levels and numbers indicate number of oscillations per burst. White, stable steady state with high (HI) and low (LI) iodide concentration. Black, chaotic oscillations. OSC, domain of period-one oscillations. (a) Setup A, (b) setup B, (c) setup C.

these two parameters affect the controlled dynamics of the CDI reaction in essentially the same fashion.

Discussion

Bursting and chaos emerge in the CDI reaction as a result of a feedback control mechanism, which regulates the flow rate and/or the ratio of input reagents. We attribute this emergence to the specific dynamic features of the CDI reaction. As mentioned above, the CDI reaction in a CSTR without feedback control exhibits two different steady states, LI and HI, bistability of LI and HI, period-one oscillations, and coexistence of period-one oscillations with HI (see Figure 9). A dynamical phase diagram similar to Figure 9a has been obtained from experimental data on the CDI reaction.[16] We suggest that the coexistence of oscillations with the HI steady state is responsible for bursting in the controlled system.

We illustrate the emergence of bursting in setups A, B, and C in Figure 9a. We assume that the oscillatory state of the system, just before the control is imposed, is characterized by point *S* and that the target concentration I_T is set to be higher than the average concentration during an oscillatory cycle but lower than in any HI steady state. Figure 9a shows how the state of the system changes during one cycle of bursting in setup A. The overall increase of the flow rate from the initial point *S* is illustrated by the arrow marked A^+. Because I_T is higher than $[I^-]$, the flow rate increases until its value is equal to that at the saddle-node (limit) point. During this increase in k_0, the oscillations remain stable. When the value of the dynamic flow rate exceeds the Hopf and limit point values, the oscillations become unstable and the system monotonically approaches the

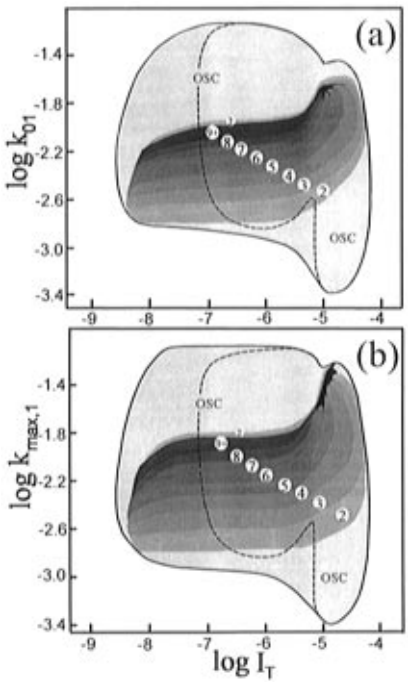

Figure 8. Bifurcation diagrams, simulations. Parameter space: (a) log k_{01} − log I_T for setup B and (b) log $k_{max,1}$ − log I_T for setup C. Lines and shaded area as in Figure 7.

HI steady state. During the approach to the HI state, the iodide concentration in the reactor exceeds I_T, which triggers a decrease of the flow rate, depicted in Figure 9a by the arrow marked A^-. To restore the oscillations, the flow rate must fall below

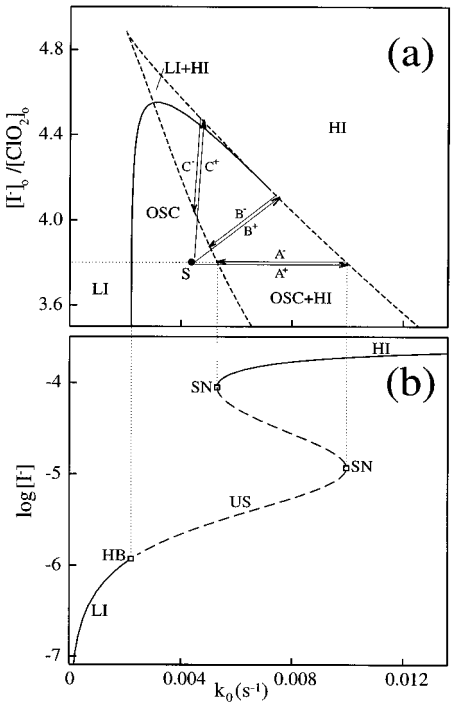

Figure 9. Bifurcation diagrams of CDI reaction in a CSTR. (a) Two-parameter diagram: solid line, Hopf bifurcation line; dashed line, saddle-node bifurcations. (b) One-parameter (solution) diagram: $[I^-]_0 = 3.8 \times 10^{-4}$ M; solid line, stable steady state; dashed line, unstable steady state. LI, low iodide steady state; HI, high iodide steady state; SN, saddle-node bifurcation point; HB, Hopf bifurcation point; US, unstable steady state; OSC, period-one oscillations. For other symbols, see text.

the value at which the HI steady state becomes unstable (leftmost dashed line in Figure 9a). In this way, bursting is produced, with a decrease of the flow rate associated with the quiescent period and an increase with the oscillatory period.

The fixed ratio $r = [I^-]_0/[ClO_2]_0$ in setup A requires that the flow rate must undergo large amplitude oscillations for the system to exhibit bursting. On the other hand, the total flow rate and the ratio r change simultaneously in setup B, as shown in Figure 9a by the arrows marked B^+ and B^-. Thus bursting in setup B requires much smaller changes in the flow rate. The path denoted in Figure 9c as C^+ and C^- represents changes in setup C during bursting oscillations. Bursting in setup C emerges from a dynamic change of the ratio r, while the total flow rate remains almost unchanged. The ratio r in setup C changes on average about twice as fast as in setup B. Therefore, we regard setup C as our most effective setup to exhibit bursting.

Unlike bursting, chaos does not seem to be directly connected with the coexistence of a stable steady state and the limit cycle oscillations. The onset of chaos occurs when the dynamic flow rate oscillates in the immediate vicinity of a Hopf bifurcation point. In the uncontrolled system, the period of oscillations is only slightly affected by the flow rate change inside the oscillatory domain, but the period increases rapidly with increasing flow rate in the vicinity of the Hopf point. For the onset of chaos in the system with feedback control, it is important that the increasing period affects predominantly the portion of a cycle with high $[I^-]$ and thus the average concentration of $[I^-]$ also changes rapidly with changing flow rate. We suggest that this strong nonlinearity is a major reason for the onset of chaos in our system.

The models (eqs 3−6) give results in good agreement with our experiments. Simple periodic and bursting behavior are the main regimes found both in experiments and simulations. Chaos, as revealed by simulations, is present only in very small parametric domains (see Figures 7 and 8). Confirmation of chaos in experiments requires more detailed study. We observed in our experiments several (up to 10) periods of period-two oscillations, but the noise, such as pulses from the peristaltic pumps and temperature fluctuations, precluded observation of further states of the period-doubling sequence. Better temperature control and more uniform delivery of the reaction mixture might allow experimental verification of the chaotic behavior.

Conclusions

We have studied three similar feedback regulation mechanisms in an attempt to explore interesting dynamical behavior in a system which, without control, displays only steady-state and/or simple periodic oscillations. We have confirmed in experiments that bursting emerges as a result of the feedback control. The characteristics of the bursting behavior—the number of spikes per burst, the frequency of spiking, and the length of the quiescent period—can easily be varied by selecting the appropriate setup and the two control parameters: the target iodide concentration I_T and the maximum flow rate k_{max}.

The dynamical behavior of the CDI reaction with feedback control is qualitatively similar to the dynamics reported for a neuron model.[11,12] Bursts of high frequency firing have special importance in brain function.[19] We have demonstrated a similar kind of dynamical activity for the "simple" inorganic reaction between chlorine dioxide and iodide, supporting the notion that chemical oscillatory systems may serve as useful dynamical models for neurons.

Acknowledgments. We thank David Bray for his help with the data acquisition and Won-kyu Han and Jana Dolnikova, Jr., for their assistance with the experiments. This work was supported by the National Science Foundation and by the W. M. Keck Foundation.

References and Notes

(1) Laplante, J. P. *J. Phys. Chem.* **1989, *93,* 3882.**
(2) Hjemfelt, A.; Ross, J. *J. Phys. Chem.* **1994**, *98*, 1176.
(3) Parmananda, P.; Eiswirth, M. *J. Phys. Chem.* **1996**, *100*, 16568.
(4) Peng, B; Petrov, V.; Showalter, K. *J. Phys. Chem.* **1991**, *95*, 4957.
(5) Petrov, V.; Gáspár, V.; Masere, J.; Showalter, K. *Nature* **1993**, *361*, 240.
(6) Schneider F. W.; Blittersdorf, R,; Förster, A.; Hauck, T.; Lebender, D.; Müller, J. *J. Phys. Chem.* **1993**, *97*, 12244.
(7) Chevalier, T.; Freund, A.; Ross, J. *J. Chem. Phys.* **1991,** *95*, 308.
(8) Dolnik, M.; Epstein, I. R. *J. Chem. Phys.* **1992**, *97*, 3265.
(9) Dolnik, M.; Epstein, I. R. *J. Chem. Phys*. **1993**, *98*, 1149.
(10) Turrigiano, G.; Abbott, L. F.; Marder, E. *Science* **1994**, *264*, 974.
(11) LeMasson, G.; Marder, E.; Abbott, L. F. *Science* **1993**, *259*, 1915.
(12) Abbott, L. F.; LeMasson, G. *Neural Computation* **1993**, *5*, 823.
(13) Siegel, M.; Marder, E.; Abbott, L. F. *Proc. Natl. Acad. Sci. U.S.A.* **1994**, *91*, 11308.
(14) Dolnik, M.; Abbott L. F.; Epstein, I. R. *J. Phys. Chem.* **1994**, *98*, 10124.
(15) Lengyel, I.; Rábai, G.; Epstein, I. R. *J. Am. Chem. Soc.* **1990**, *112*, 9104.
(16) Lengyel, I; Li, J.; Epstein, I. R. *J. Phys. Chem.* **1992**, *96*, 7033.
(17) Handbook of Preparative Inorganic Chemistry, 2nd ed.; Brauer, G., Ed.; Academic Press: NY, 1963; Vol. 1, p 301.
(18) Marek, M.; Schreiber, I. *Chaotic Behavior of Deterministic Dissipative Systems*; Cambridge University: Cambridge, 1991.
(19) Lisman, J. E. *Trends Neurosci.* **1997**, *20*, 38.